Computational Study of Small Molecule Binding for Both Tethered and Free Conditions

F. Marty Ytreberg*

Department of Physics, University of Idaho, Moscow, Idaho 83844-0903

Received: December 10, 2009; Revised Manuscript Received: March 5, 2010

Using a calix[4]arene-benzene complex as a test system, we compare the potential of mean force for when the calix[4]arene is tethered versus free. When the complex is in vacuum, our results show that the difference between tethered and free is primarily due to the entropic contribution to the potential of mean force resulting in a significant binding free energy difference of 6.6 kJ/mol. By contrast, when the complex is in water, our results suggest that there is no appreciable difference between tethered and free. This study elucidates the roles of entropy and enthalpy for this small molecule system and emphasizes the point that tethering the receptor has the potential to dramatically impact the binding properties. These findings should be taken into consideration when using calixarene molecules in nanosensor design.

Introduction

Calixarenes are macrocycles that are of interest due to the fact that they can be easily synthesized and can be functionalized to selectively bind neutral or ionic analytes (see reviews in refs 1−5). One use for calixarenes that is of specific interest to the current study is in nanosensor design (e.g., refs 6−9). Calixarenes are typically used in nanosensors by coating the nanomaterial with gold and then tethering the calixarenes to the gold. Note that this requires the calixarenes to have sulfur atoms, which has been the focus of some previous experimental studies.[10,11]

A reasonable question that is also the motivation for our study is, How does tethering calixarene to a surface affect the binding properties of the calixarene to analytes? This is an important question considering that a researcher may only have knowledge of binding properties for free (i.e., not tethered) conditions. There are previous computational studies of calixarenes that have focused on understanding mechanisms for calixarene binding, primarily to ions (e.g., refs 12−17). However, we are not aware of any previous study that has addressed the question of how tethering calixarenes affects their binding properties.

For the current study we compare the effects of tethering a calix[4]arene on the binding properties both in vacuum and in water. Note that the "[4]" means that there are four aromatic rings in the structure. We computed the potential of mean force (PMF) for calix[4]arene-benzene binding for four cases: (i) in vacuum with the calix[4]arene tethered; (ii) in vacuum with the calix[4]arene free (i.e., not tethered); (iii) in water with the calix[4]arene tethered; and (iv) in water with the calix[4]arene free. Our results below show that, when the complex is in vacuum, the difference between tethered and free is due primarily to the entropic contribution to the potential of mean force, resulting in a significant binding free energy difference of 6.6 kJ/mol. By contrast, when the complex is in water, our results suggest that the difference between tethered and free is due entirely to the enthalpic contribution, resulting in a negligible (considering the confidence interval) binding free energy difference of 1.6 kJ/mol.

* E-mail: ytreberg@uidaho.edu.

Computational Methods

The initial structure for the calix[4]arene−benzene complex was obtained from experimental X-ray crystallography (personal communication from Pam Shapiro's lab at University of Idaho). The necessary simulation topologies for both the calix[4]arene and benzene were then generated by the PRODRG server.[18] We then modified the partial charges to be consistent with the GROMOS-96 43A1 forcefield,[19] e.g., all CH_3 groups were set to zero partial charge. The GROMACS simulation package version 3.3.3[20] was used for all molecular dynamics simulations described below with the default GROMOS-96 43A1 forcefield.[19]

For the vacuum simulations, the calix[4]arene-benzene complex was first minimized using the steepest descent for 1000 steps. For subsequent production simulations, all van der Waals and electrostatic interactions were computed, i.e., no cutoffs were used. A time step of 1.0 fs was utilized with no constraints. The temperature was maintained at a constant value using Langevin dynamics[21] with a friction coefficient of 1.0 amu/ps.

For the simulations in water, the calix[4]arene−benzene complex was solvated in a cubic box of SPC water[22] of approximate initial size 4.5 nm per side. The system was then minimized using the steepest descent for 1000 steps. To allow for some equilibration of the water, the system was then simulated for 100 ps with the positions of all heavy atoms in the complex harmonically restrained with a force constant of 1000 kJ/mol/nm^2. For this equilibration simulation, the pressure was maintained at 1.0 atm using the Berendsen algorithm.[23] Subsequent production simulations were carried out with the volume fixed at the final value from the equilibration. For all water simulations, the LINCS algorithm[24] was used to constrain hydrogens to their ideal lengths allowing the use of a 2.0 fs time step. The temperature was maintained at a constant value using Langevin dynamics[21] with a friction coefficient of 1.0 amu/ps. Particle mesh Ewald[25] was used for electrostatics with a real-space cutoff of 1.0 nm and a Fourier spacing of 0.1 nm. van der Waals interactions used a cutoff with a smoothing function such that the interactions smoothly decayed to zero between 0.75 and 0.9 nm. Dispersion corrections for the energy and pressure were utilized.[26]

To perform the tethered simulations both in vacuum and in water, we harmonically restrained the two sulfur atoms to their

10.1021/jp911704n
Published on Web 04/06/2010

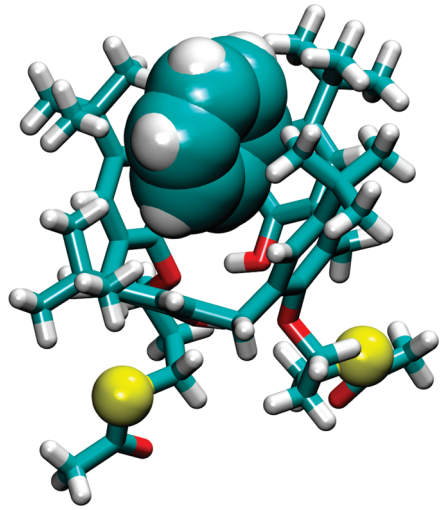

Figure 1. The calix[4]arene−benzene system used for the current study. The calix[4]arene molecule is characterized by a wider upper rim, which provides a binding pocket, and a narrow lower rim. The two sulfur atoms are shown in a larger size and allow the calix[4]arene to be tethered to a gold surface. The difference between the tethered and free simulations in the current study is that these sulfur atoms were harmonically restrained to their initial Cartesian coordinate positions during the tethered simulations but were not restrained for the free simulations. This image was generated using VMD.[32]

absolute Cartesian coordinate positions (see Figure 1) using a force constant of 10 000 kJ/mol/nm^2. Thus, for the tethered simulations, the sulfur atoms were not allowed to move significantly from their positions given at the end of the equilibration simulations. The purpose is to mimic the effect of the calix[4]arene binding to a gold surface. This harmonic restraint on the sulfur atoms was not present for the free simulations. Given the strength of the sulfur restraints, one may worry that the appropriate temperature distribution will not be maintained, especially in vacuum. Thus we calculated the simulation temperatures and found that, in all cases, the average temperatures were within 2.0 K of the target value.

Generating PMF Estimates. We computed all PMFs using umbrella sampling and weighted histogram analysis (WHAM).[27] Our technique for estimating the PMF using WHAM is described in ref 28. Briefly, the GROMACS 3.3.3 software package[20] was modified to provide a harmonic biasing potential $U_r(r) = 0.5k_r(r - r_0)^2$, which depends only on the center of mass separation r between the calix[4]arene and the benzene. For all PMF estimates, we used a total of 33 windows $r_0 =$ 0.40, 0.45, 0.50, ..., 1.95, 2.00 nm. Histograms of the harmonic biasing potential energy necessary for the WHAM analysis were generated using 200 bins of width 0.008 nm. For the vacuum system, each window was simulated for 32.0 ns; 16.0 ns were discarded for equilibration, and 16.0 ns were used for the WHAM analysis. For the water system, each window was simulated for 4.0 ns; 2.0 ns were discarded for equilibration, and 2.0 ns were used for the analysis. For all PMF estimates below the biasing potential, U_r used a force constant $k_r = 3000$ kJ/mol/nm^2, and the estimates include the $2\ln(r)$ Jacobian correction.[28,29]

Note that, for the simulations of the complex in water, the system size prevents the long simulation times necessary to obtain converged PMFs without additional restraints. Thus, for the water simulations (but not for the vacuum simulations) we utilized an axial restraint that keeps the benzene on the binding axis relative to the calix[4]arene as described in ref 28. Use of this restraint means that it is not valid to directly compare the vacuum and water PMFs. However, it is still valid to compare the tethered and free conditions for water, which is the purpose of this study.

To ensure that the simulation times for each window allowed adequate sampling of the rotational and translational degrees of freedom, we computed diffusion constants and correlations times. The rotational correlation time for the calix[4]arene was approximately 30 ps in vacuum and 150 ps in water. Thus, for the water system, each umbrella sampling window is simulated over 25 times longer than the corresponding rotational correlation time. The diffusion constant for calix[4]arene was approximately 2×10^{-5} cm^2/s in vacuum and 0.5×10^{-5} cm^2/s in water. Thus, for the water system, each window has a diffusion length of approximately 2 nm^2.

Estimating Entropic and Enthalpic Contributions. To estimate the entropic contribution to the PMF $T\Delta S(r)$, we used the fact that the entropy is related to the derivative of the PMF $\Delta G(r)$ with respect to system temperature T (see also refs 30 and 31),

$$T\Delta S(r) = -T\left(\frac{\partial \Delta G(r,T)}{\partial T}\right) \quad (1)$$

This derivative was numerically estimated by computing the PMF at three temperatures 270, 300, and 330 K and then using a three-point finite difference approximation. The enthalpic contribution $\Delta H(r)$ was then estimated via

$$\Delta H(r) = \Delta G(r) + T\Delta S(r) \quad (2)$$

Uncertainty Estimation. The uncertainty for ΔG, $T\Delta S$, and ΔH were estimated by computing the 95% confidence interval (i.e., two times the standard error) over independent trials. Independent trials were generated using the same starting configuration but with different random number generator seeds. For both the tethered and free conditions in vacuum, 10 independent estimates of the PMF were generated at each of the three temperatures (i.e., 30 PMF estimates tethered and 30 free). For both the tethered and free conditions in water, five independent estimates of the PMF were generated at each of the three temperatures (i.e., 15 PMF estimates tethered and 15 free).

Results and Discussion

The PMF results for both vacuum and water simulations for all three temperatures are shown in Figure 2. These results were used to compute the entropic and enthalpic contributions to the PMF shown in Figure 3. The binding free energy differences between tethered and free conditions $\Delta\Delta G_{bind}$ for vacuum and water were obtained by numerically integrating the $\Delta G(r)$ curves from $r = 0.4$ to $r = 2.0$ nm. The entropic and enthalpic contributions to the PMF were computed using eqs 1 and 2.

Results for the calix[4]arene−benzene complex in vacuum are shown in Figure 3a and reveal two major differences between the free and tethered conditions. First, when the PMF plateaus ($r > 1.5$ nm), both the entropic and enthalpic contributions for the free conditions are larger than those for the tethered. Note that the free entropic contribution is larger than that of the tethered by approximately 15 kJ/mol, and the enthalpic contribution is larger by about 8 kJ/mol. Thus, it is primarily the entropic difference between free and tethered that leads to the more favorable binding for tethered conditions. The second difference between free and tethered conditions occurs at $r \approx$

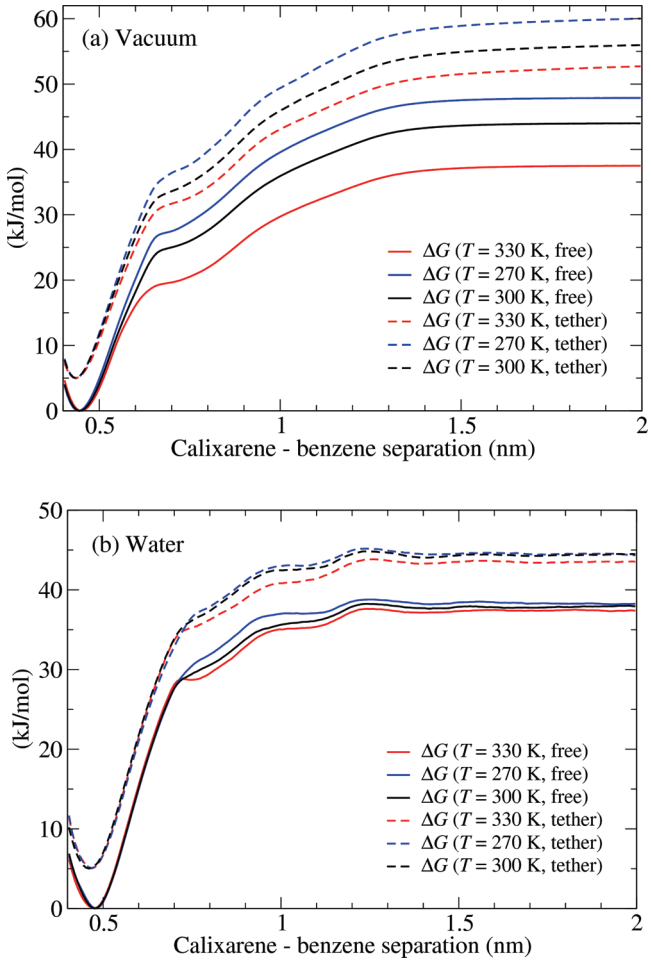

Figure 2. The calix[4]arene−benzene PMF for three different temperatures: 270 K (blue), 300 K (black), and 330 K (red). Both tethered (dashed line) and free (solid line) conditions are shown. The tethered condition results are shifted by 5 kJ/mol to separate the free and tethered sets of curves.

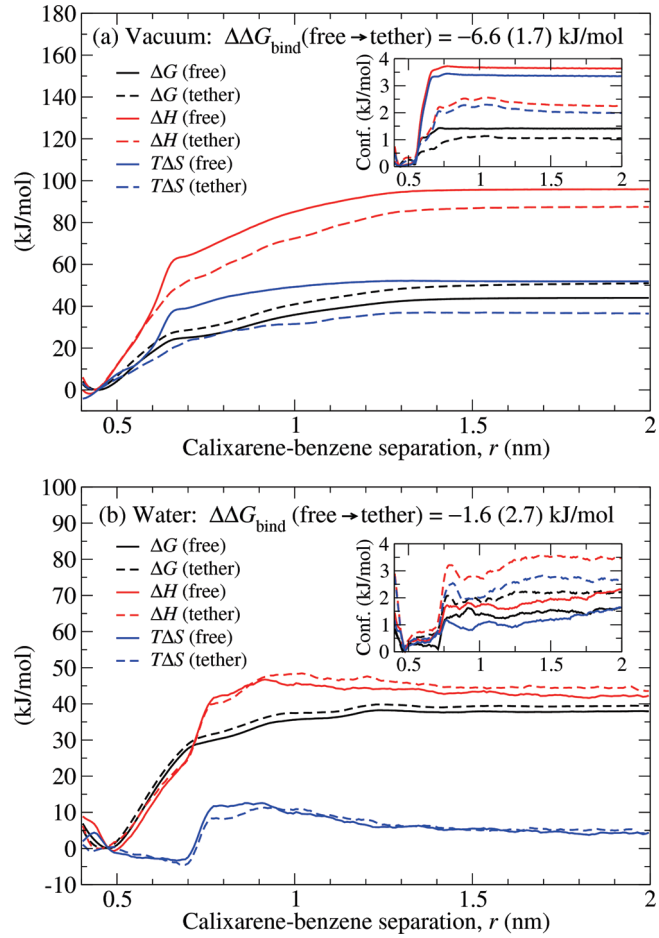

Figure 3. The calix[4]arene−benzene PMF (black) at 300 K showing the enthalpic (red) and entropic (blue) contributions. Both tethered (dashed line) and free (solid line) conditions are shown. The $\Delta\Delta G_{bind}$ values show the difference between the binding free energy for tethered and free conditions with the 95% confidence interval shown in parentheses obtained by performing multiple independent simulations. Curves show the average values and the insets show the 95% confidence intervals for the corresponding average. (a) Simulation results in vacuum. (b) Simulation results in water.

0.6 nm where the entropic and enthalpic contributions to the PMF increase dramatically for free as compared to tethered conditions. This difference can be understood by noting that the benzene is at the (wider) upper rim of the binding pocket at $r \approx 0.6$ nm (see Figure 1), and just outside the pocket at $r \approx 0.7$ nm where entropic and enthalpic contributions for the free condition have a narrow flat region. We believe that this difference between the free and tethered can be attributed to the fact that the tethering of the calix[4]arene provides a more rigid binding pocket than under free conditions leading to a sharp increase in entropy under free conditions as the benzene reaches the outer edge of the pocket.

To test our prediction that the binding pocket is more rigid under tethered conditions than free, we computed the root-mean-square fluctuations for the calix[4]arene atoms. Figure 4 shows the difference in the fluctuations between tethered and free conditions. These results suggests that the binding pocket is indeed more rigid under tethered conditions due primarily to the two *t*-butyl groups that are furthest from the sulfur atoms; the other two *t*-butyl groups nearest the sulfur atoms show a small but consistent decrease in fluctuation.

Our vacuum results suggest that the free energy of binding under tethered conditions is more favorable than free by $\Delta\Delta G_{bind} = -6.6$ kJ/mol with a 95% confidence interval of 1.7 kJ/mol, due primarily to the entropic contribution to the PMF. Thus, if one wishes to design a gas phase nanosensor using calix[4]arenes, we strongly suggest testing the binding properties under tethered conditions.

Results for the calix[4]arene-benzene complex in water are shown in Figure 3b. The results suggest that there is no appreciable difference (considering the confidence interval) between tethered and free. Apparently the entropy of the water molecules completely counters the entropy-dominant effects seen in the vacuum system. We believe this is attributed to the fact that the effective volume available to the water molecules is reduced when the benzene is completely dissociated from the calix[4]arene; this also leads to the entropy decrease observed in the PMFs for both tethered and free between $r \approx 0.9$ and $r \approx 1.5$ nm.

Note that we do not expect that our results are completely general, and thus different receptor−compound complexes will likely lead to differences from our results above. However, this does not change our general conclusion that one should test binding properties under the desired conditions.

Conclusion

We have studied the effects of tethering on small molecule binding properties using a calix[4]arene−benzene complex as

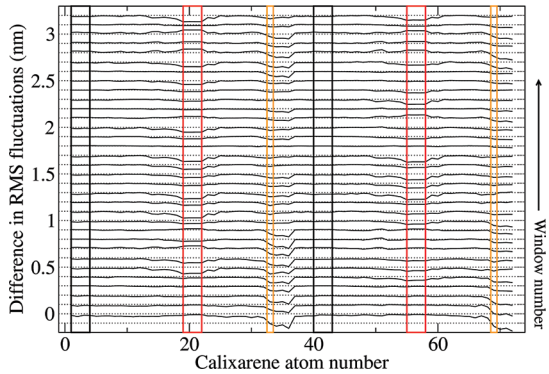

Figure 4. Difference between the root-mean-square fluctuation between tethered and free for calix[4]arene atoms in vacuum. Regions of the curves that fall below the dotted horizontal lines indicate decreased fluctuations under tethered conditions as compared to free. Results are shown for all 33 umbrella sampling windows, i.e., the bottom curve corresponds to $r_0 = 0.4$ nm and the top corresponds to $r_0 = 2.0$ nm. The yellow boxes show the two sulfur atoms that were restrained during the tethered simulations. The black boxes show the two *t*-butyl $C(CH3)_3$ groups located on the upper rim that are nearest the sulfur, and the red boxes show the two *t*-butyl groups furthest from the sulfur (see Figure 1).

a test system. Simulations of the complex in vacuum and in water were performed and the PMF curves were computed and compared for tethered and free conditions.

Our results for the calix[4]arene−benzene complex in vacuum show that the primary difference between free and tethered conditions is the entropic contribution to the PMF. Thus, in vacuum, the free energy of binding under tethered conditions is more favorable than free by $\Delta\Delta G_{bind} = -6.6$ kJ/mol. By contrast, when the calix[4]arene complex is in water, there is no appreciable difference between free and tethered conditions.

This study elucidates the roles of entropy and enthalpy under tethered and free conditions both in vacuum and in water. Our general conclusion is a reminder that, if one wishes to design a gas phase or aqueous nanosensor using calix[4]arenes, we suggest that the binding properties of the calix[4]arene should be tested under conditions relevant to the sensor.

Acknowledgment. The author thanks Pam Shapiro and Steven Hung for providing the experimental structure for the calix[4]arene−benzene complex, and Conrad Shyu for helpful discussion. The project described was supported by Award Numbers P20RR016448 and R21GM083827 from the National Institutes of Health. The content is soley the responsibility of the authors and does not necessarily represent the official views of the National Institutes of Health. The research was also supported by Idaho NSF-EPSCoR, and by IBEST and BANTech at the University of Idaho.

References and Notes

(1) de Namor, A.; Cleverley, R.; Zapata-Ormachea, M. *Chem. Rev.* **1998**, *98*, 2495–2526.
(2) Schatz, J. *Collect. Czech. Chem. C* **2004**, *69*, 1169–1194.
(3) Ludwig, R. *Microchim. Acta* **2005**, *152*, 1–19.
(4) Jose, P.; Menon, S. *Bioinorg. Chem. Appl.* **2007**, *2007*, 65815−1–16.
(5) Sameni, S.; Jeunesse, C.; Matt, D.; Harrowfield, J. *Chem. Soc. Rev.* **2009**, *38*, 2117–2146.
(6) Filenko, D.; Gotszalk, T.; Kazantseva, Z.; Rabinovych, O.; Koshets, I.; Shirshov, Y.; Kalchenko, V.; Rangelow, I. *Sensor. Actuat. B-Chem.* **2005**, *111*, 264–270.
(7) Koshets, I.; Kazantseva, Z.; Shirshov, Y.; Cherenok, S.; Kalchenko, V. *Sensor. Actuat. B-Chem.* **2005**, *106*, 177–181.
(8) Chen, L.; He, X.; Hu, X.; Xu, H. *Analyst* **1999**, *124*, 1787–1790.
(9) Dickert, F.; Schuster, O. *Microchim. Acta* **1995**, *119*, 55–62.
(10) Sone, T.; Ohba, Y.; Moriya, K.; Kumada, H.; Ito, K. *Tetrahedron* **1997**, *53*, 10689–10698.
(11) Nakayama, J.; Katano, N.; Sugihara, Y.; Ishii, A. *Chem. Lett.* **1997**, *26*, 897–898.
(12) Bohmer, V.; Dorrenbacher, R.; Frings, M.; Heydenreich, M.; de Paoli, D.; Vogt, W.; Ferguson, G.; Thondorf, I. *J. Org. Chem.* **1996**, *61*, 549–559.
(13) Den Otter, W. K.; Briels, W. J. *J. Chem. Phys.* **1997**, *107*, 4968–4978.
(14) Golebiowski, J.; Lamare, V.; Martins-Costa, M. T. C.; Millot, C.; Ruiz-Lopez, M. F. *Chem. Phys.* **2001**, *272*, 47–59.
(15) Ghoufi, A.; Malfreyt, P. *J. Chem. Phys.* **2006**, *125*, 224503−1–12.
(16) Rodríguez-Ropero, F.; Zanuy, D.; Aleman, C. *J. Comput. Chem.* **2007**, *29*, 1233–1241.
(17) Venkataramanan, N. S.; Sahara, R.; Mizuseki, H.; Kawazoe, Y. *J. Phys. Chem. C* **2008**, *112*, 19676–19679.
(18) Schüttelkopf, A. W.; van Aalten, D. M. F. *Acta Crystallogr., Sect. D* **2004**, *60*, 1355–1363.
(19) van Gunsteren, W. F.; Billeter, S. R.; Eising, A. A.; Hünenberger, P. H.; Krüger, P.; Mark, A. E.; Scott, W. R. P.; Tironi, I. G. *Biomolecular Simulation: The GROMOS96 Manual and User Guide*; Hochschulverlag: Zurich, Switzerland, 1996.
(20) Van Der Spoel, D.; Lindahl, E.; Hess, B.; Groenhof, G.; Mark, A. E.; Berendsen, H. J. C. *J. Comput. Chem.* **2005**, *26*, 1701–1718.
(21) van Gunsteren, W. F.; Berendsen, H. J. C.; Rullmann, J. A. C. *Mol. Phys.* **1981**, *44*, 69–95.
(22) Berendsen, H. J. C.; Postma, J. P. M.; van Gunsteren, W. F.; Hermans, J. *Intermolecular Forces*; Reidel: Dordrecht, The Netherlands, 1981; pp 331−342.
(23) Berendsen, H. J. C.; Postma, J. P. M.; van Gunsteren, W. F.; DiNola, A.; Haak, J. R. *J. Chem. Phys.* **1984**, *81*, 3684–3690.
(24) Hess, B.; Bekker, H.; Berendsen, H. J. C.; Fraaije, J. G. E. M. *J. Comput. Chem.* **1997**, *18*, 1463–1472.
(25) Darden, T.; York, D.; Pedersen, L. *J. Chem. Phys.* **1993**, *98*, 10089–10092.
(26) Allen, M. P.; Tildesley, D. J. *Computer Simulation of Liquids*; Oxford University Press: New York, 1989.
(27) Kumar, S.; Rosenberg, J. M.; Bouzida, D.; Swendsen, R. H.; Kollman, P. A. *J. Comput. Chem.* **1992**, *13*, 1011–1021.
(28) Ytreberg, F. M. *J. Chem. Phys.* **2009**, *130*, 164906−1–8.
(29) Trzesniak, D.; Kunz, A.-P. E.; van Gunsteren, W. F. *Chem. Phys. Chem.* **2007**, *8*, 162–169.
(30) Ghosh, T.; García, A. E.; Garde, S. *J. Chem. Phys.* **2002**, *116*, 2480–2486.
(31) Choudhury, N.; Pettitt, B. M. *J. Phys. Chem. B* **2006**, *110*, 8459–8463.
(32) Humphrey, W.; Dalke, A.; Schulten, K. *J. Mol. Graph. Model.* **1996**, *14*, 33–38.

JP911704N